



A catalogue of white dwarf candidates in VST ATLAS

Nicola Pietro Gentile Fusillo,¹★ Roberto Raddi,¹ Boris T. Gänsicke,¹ J. J. Hermes,²†
Anna F. Pala,¹ Joshua T. Fuchs,² Ben Chehade,³ Nigel Metcalfe³ and Tom Shanks³

¹Department of Physics, University of Warwick, Coventry CV4 7AL, UK

²University of North Carolina, Chapel Hill, NC 27599-3255, USA

³Department of Physics, Durham University, South Road, Durham DH1 3LE, UK

Accepted 2017 March 24. Received 2017 March 23; in original form 2017 January 21

ABSTRACT

The Sloan Digital Sky Survey (SDSS) has created a knowledge gap between the Northern and the Southern hemispheres, which is very marked for white dwarfs: Only $\simeq 15$ per cent of the known white dwarfs are south of the equator. Here, we make use of the VLT Survey Telescope (VST) ATLAS survey, one of the first surveys obtaining deep, optical, multiband photometry over a large area of the southern skies, to remedy this situation. Applying the colour and proper-motion selection developed in our previous work on SDSS to the most recent internal data release (2016 April 25) of VST ATLAS, we created a catalogue of $\simeq 4200$ moderately bright ($g \leq 19$), high-confidence southern white dwarf candidates, which can be followed up individually with both the large array of southern telescopes or in bulk with ESO's forthcoming multi-object spectrograph 4MOST.

Key words: catalogues – surveys – proper motions – white dwarfs.

1 INTRODUCTION

White dwarfs are the final stage of the evolution of stars with main sequence masses $M > 0.8$ and $M \lesssim 8\text{--}10 M_{\odot}$ (Iben, Ritossa & Garcia-Berro 1997), a range that includes the vast majority of all stars. White dwarfs are therefore key tracers of the evolutionary history of the Galaxy (e.g. Torres et al. 2005; Tremblay et al. 2014) and significant contributors to the global stellar population. However, to fully exploit the diagnostic potential of the Galactic white dwarf population, it is necessary to reliably constrain fundamental parameters such as their space density (Holberg, Oswalt & Sion 2002; Holberg et al. 2008; Giammichele, Bergeron & Dufour 2012; Sion et al. 2014), mass distribution (Bergeron, Saffer & Liebert 1992; Liebert, Bergeron & Holberg 2005; Falcon et al. 2010; Tremblay et al. 2013, 2016) and luminosity function (Catalán et al. 2008; Giammichele et al. 2012; Rebassa-Mansergas et al. 2015). These studies require large, homogeneous and well-defined samples that, given the intrinsic low luminosity of white dwarfs, are still challenging to be assembled.

Large samples of white dwarfs are also the starting point in searches for rare sub-types like magnetic white dwarfs (Gänsicke, Euchner & Jordan 2002; Schmidt et al. 2003; Külebi et al. 2009; Kepler et al. 2013; Hollands, Gänsicke & Koester 2015), pulsating white dwarfs (Castanheira et al. 2004; Greiss et al. 2014; Gentile Fusillo, Hermes & Gänsicke 2016, see Section 6.4),

high/low mass white dwarfs (Vennes & Kawka 2008; Brown et al. 2010; Hermes et al. 2014), white dwarfs with unresolved low mass companions (Farihi, Becklin & Zuckerman 2005; Girven et al. 2011; Steele et al. 2013), white dwarfs with rare atmospheric composition (Schmidt et al. 1999; Dufour et al. 2010; Gänsicke et al. 2010; Kepler, Koester & Orique 2016), close white dwarf binaries (Marsh, Nelemans & Steeghs 2004; Parsons et al. 2011), metal polluted white dwarfs (Sion, Leckenby & Szkody 1990; Zuckerman & Reid 1998; Dufour et al. 2007; Koester, Gänsicke & Farihi 2014; Raddi et al. 2015) or white dwarfs with dusty or gaseous planetary debris discs (Gänsicke et al. 2006; Farihi, Jura & Zuckerman 2009; Debes et al. 2011; Wilson et al. 2014; Manser et al. 2016).

In recent years, the number of known white dwarfs has increased by an order of magnitude, in particular thanks to the Sloan Digital Sky Survey (SDSS, York et al. 2000) that led to the identification of over 26 000 white dwarfs mainly in the Northern hemisphere (Harris et al. 2003; Eisenstein et al. 2006; Kleinman et al. 2013; Kepler et al. 2015; Gentile Fusillo, Gänsicke & Greiss 2015a; Kepler et al. 2016). The Southern hemisphere (below Dec. $\simeq -20^{\circ}$) has not yet been surveyed by deep multicolour CCD photometric surveys, and consequently only ≈ 15 per cent of all known white dwarfs are south of the celestial equator (cf. Fig. 1). However, the potential for identifying large numbers of white dwarfs in the Southern hemisphere is now rapidly growing thanks to the public surveys carried out by the European Southern Observatory (ESO) with the Very Large Telescope (VLT) Survey Telescope (VST; Schipani et al. 2012): ATLAS (Shanks et al. 2015), VPHAS+ (Drew et al. 2014) and KIDS (de Jong et al. 2013). In a pilot study, we have identified white dwarfs at low Galactic latitudes by applying

* E-mail: n.gentile-fusillo@warwick.ac.uk

† Hubble Fellow.

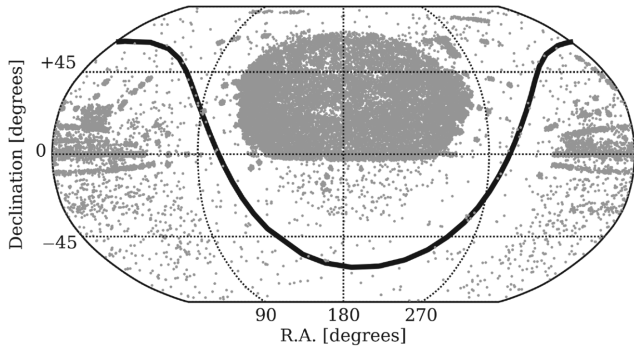


Figure 1. Sky distribution of the $\sim 39\,000$ white dwarfs confirmed to date. Only ~ 15 per cent of them are located below the equator.

Table 1. Summary of the white dwarf candidate selection in ATLAS.

ATLAS objects in initial colour cut	12 359
Of which with no proper motion	952
Magnitude limit of final sample	$g \leq 19$
Final sample of white dwarf candidates (Section 5)	11 407
High confidence white dwarf candidates ($P_{WD} \geq 0.41$)	~ 4200
Also in Gentile Fusillo et al. (2015a) catalogue	
of SDSS white dwarf candidates	879
Of which confirmed white dwarfs	130
Of which confirmed contaminants	171

traditional colour-cuts to VPHAS+ photometry (Raddi et al. 2016). Here, we present a catalogue of 11 407 colour-selected sources from ATLAS for which we calculated *probabilities of being white dwarfs* (P_{WD}) according to the method described in Gentile Fusillo et al. (2015a). The P_{WD} values allow for selection of ATLAS white dwarf candidates with flexible efficiency and completeness, from which we estimate the catalogue to contain ~ 4100 genuine white dwarfs (Table 1).

In the following two sections, we briefly summarize the ATLAS survey and describe the properties of the photometric system, and how it compares to SDSS photometry. In Section 4, we briefly outline the methodology used to combine photometry and proper motions to calculate P_{WD} values. The catalogue of white dwarf candidates is presented in Section 5. The completeness of the catalogue and the spectroscopic confirmation of some white dwarf candidates are discussed in Section 6. The last section is dedicated to our conclusions.

2 VST ATLAS

VST ATLAS is primarily a cosmology-focused survey aiming to image 4700 deg^2 of the Southern Sky at high galactic latitudes ($|b| > 30^\circ$) in five bands (*ugriz*) to comparable depths to the SDSS in the north. The ATLAS footprint is divided into two contiguous blocks in the North and South Galactic Caps (NGC, SGC). The ATLAS SGC area lies in the ranges $21^{\text{h}}30^{\text{m}} < \text{RA} < 04^{\text{h}}00^{\text{m}}$ and $-40^\circ < \text{Dec.} < -10^\circ$, whilst the NGC area lies in the ranges $10^{\text{h}}00^{\text{m}} < \text{RA} < 15^{\text{h}}30^{\text{m}}$ and $-20^\circ < \text{Dec.} < -2.5^\circ$ plus $10^{\text{h}}00^{\text{m}} < \text{RA} < 15^{\text{h}}00^{\text{m}}$ and $-30^\circ < \text{Dec.} < -20^\circ$ (Fig. 2).

The survey is carried out at the 2.6-m VST, located at Cerro Paranal in Chile. The telescope mounts at the prime focus a 1 deg^2 wide imaging instrument, the OmegaCAM (Kuijken 2011), which consists of 32 CCDs of $4\text{k} \times 2\text{k}$ pixels each. The narrow gaps between the individual CCDs allow for an overall geometric filling

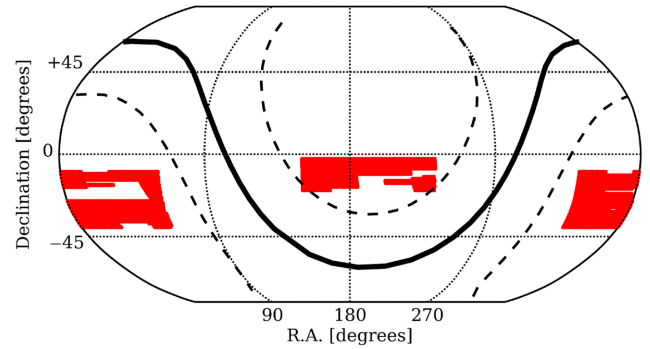


Figure 2. Footprint of the sky area covered in all five filters (*ugriz*) by ATLAS at the time of the internal data release of 2016 April 25. The solid black line indicates the location of the galactic plane and the dashed lines indicate regions $\pm 30^\circ$ from it.

factor of 91.4 per cent (see Shanks et al. 2015, for more details). The ATLAS band-passes are similar to those of the SDSS filters. Observations are taken in pairs for each filter and exposure times of 60 s for *u*, 50 s for *g* and 45 s for *r*, *i* and *z*. The imaging data is reduced by the Cambridge Astronomical Survey Unit using the VST data flow software. Images are trimmed and de-biased using nightly calibration frames and then flat-fielded using accumulated monthly stacked twilight sky flats. The frames are then corrected for cross-talk and de-fringed, if necessary. The resulting imaging data comprise the combination of the two individual images for each of the original CCDs (Shanks et al. 2015). For the analysis presented here, we used the latest internal data release available on 2016 April 25. This release includes coverage in all five filters and photometric quality flags for $\sim 2400 \text{ deg}^2$ of the sky, surpassing the publicly available Data Release 3.

3 ATLAS VERSUS SDSS

VST ATLAS uses the same optical filters as SDSS (*ugriz*) and in many ways aims to be the Southern hemisphere counterpart of SDSS. However, though the filter systems are nominally the same, the actual filter transmission curves have small differences, the detectors are not the same, the observing conditions at the telescope sites are different, and the flux calibration is conducted in different ways. As a result, ATLAS and SDSS magnitudes, and therefore colours, are not perfectly equivalent. As part of their re-calibration of ATLAS photometry to the AB system, Shanks et al. (2015) carried out a detailed comparison of SDSS and ATLAS photometry. ATLAS and SDSS overlap over an equatorial region of $\sim 300 \text{ deg}^2$ covering parts of both the NGC ($10^{\text{h}} \lesssim \text{RA} \lesssim 15^{\text{h}}30^{\text{m}}$; $-3.5^\circ \lesssim \text{Dec.} \lesssim -2^\circ$) and the SGC ($22^{\text{h}}40^{\text{m}} \lesssim \text{RA} \lesssim 3^{\text{h}}$; $-11^\circ \lesssim \text{Dec.} \lesssim -9^\circ$). Shanks et al. (2015) used the objects in the NGC overlapping region to develop a set of colour-dependent equations to convert ATLAS (AB) magnitude in equivalent SDSS magnitudes:

$$\begin{aligned}
 u_{\text{SDSS}} &= u_{\text{ATLAS}} + 0.01 \times (u - g) + 0.27, \\
 g_{\text{SDSS}} &= g_{\text{ATLAS}} + 0.05 \times (g - r) - 0.06, \\
 r_{\text{SDSS}} &= r_{\text{ATLAS}} + 0.03 \times (g - r) - 0.035, \\
 i_{\text{SDSS}} &= i_{\text{ATLAS}} - 0.025, \\
 z_{\text{SDSS}} &= z_{\text{ATLAS}} - 0.04 \times (i - z) + 0.04.
 \end{aligned} \tag{1}$$

Since our selection method for white dwarf candidates makes use of a probability map in reduced proper motion–colour space that was initially developed from SDSS data (see Section 5), it is of

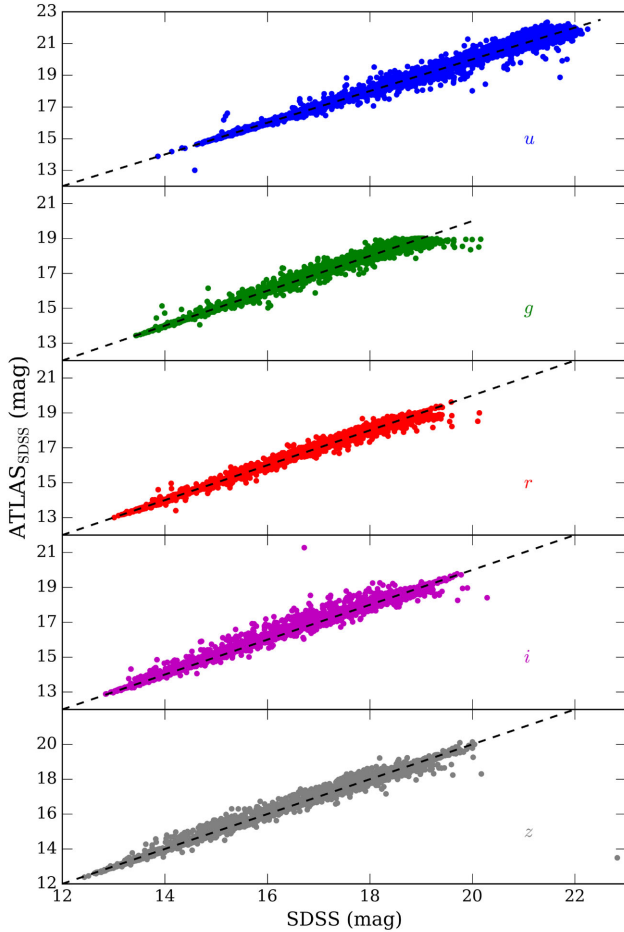


Figure 3. Comparison of ATLAS_{SDSS} and SDSS magnitudes for a sample of $\approx 112\,000$ point sources. The dashed black lines indicate a 1:1 relationship. The comparison objects were chosen as SDSS objects with clean photometry.

paramount importance to have reliable SDSS-equivalent ATLAS magnitudes (ATLAS_{SDSS} from here on). In order to evaluate the robustness of the magnitude transformations developed by Shanks et al. (2015), in particular their applicability to blue objects, we carried out some further comparison with SDSS. We retrieved the available SDSS photometry of all ATLAS sources in the overlapping regions with clean $g \leq 19.5$ SDSS photometry ($\approx 112\,000$ objects). We then applied equation (1) to the ATLAS photometry and compared the ATLAS_{SDSS} magnitudes with the SDSS ones (Fig. 3). We find that the mean values of SDSS–ATLAS_{SDSS} magnitudes for the objects in our overlapping samples are: $u = 0.0109 \pm 0.0003$, $g = 0.0089 \pm 0.0001$, $r = 0.0086 \pm 0.0001$, $i = 0.0098 \pm 0.0002$, $z = 0.011 \pm 0.0003$. These mean differences are smaller than the typical uncertainties in the SDSS and ATLAS magnitude. We therefore conclude that ATLAS_{SDSS} magnitudes are, for most intents and purposes, equivalent to SDSS ones, and our selection method for white dwarf candidates (Gentile Fusillo et al. 2015a) can be directly applied to them.

4 COLOUR SELECTION AND PROPER MOTIONS

Using the free form SQL query tool available on the OmegaCAM Science Archive webpage, we retrieved photometry for all ATLAS

sources that have been observed in all five filters, marked as ‘stellar’ or ‘probable stellar’ and with no ‘important’¹ quality issue (Table 2). We then applied the magnitude conversions described by equation (1) to calculate ATLAS_{SDSS} magnitudes for all our sources. The first step in our photometric selection method for white dwarf candidates involves applying a set of colour constraints that broadly select all blue sources (Table 3). These colour-cuts are designed to include all white dwarfs with $T_{\text{eff}} \gtrsim 7000$ K and are required to reduce the initial sample to a more manageable size, but they are not sufficient to eliminate contamination from QSO and other blue objects (i.e. sub-dwarfs, A stars; for more details see Gentile Fusillo et al. 2015a). This initial broad colour selection resulted in a sample of 12 359 blue ATLAS sources. ATLAS does not provide proper-motion measurements, thus we decided to retrieve those from the recently published Absolute Proper motions Outside the Plane (APOP, Qi et al. 2015) catalogue. APOP proper motions are calculated from carefully re-reduced photographic plates from the STScI Catalog of Objects and Measured Parameters from All-Sky Surveys (COMPASS) archive of the GSC-II project (Lasker & STScI Sky-Survey Team 1998). APOP covers $22\,525\text{ deg}^2$ and provides proper motions for 100 774 153 objects to the limiting magnitude of $R \approx 20.8$ with typical uncertainties ranging between 4 and 9 mas yr^{−1}. However, the astrometry of APOP and ATLAS corresponds to observations taken several years apart and most white dwarfs have high proper motions, typically ranging from 20 to 200 mas yr^{−1}. White dwarfs can therefore move significantly over a few years to decades and a simple cross match between ATLAS and APOP using a fixed matching radius can easily lead to several mis-matches or missing objects.

We therefore divided our cross-matching procedure in three separate steps. For each ATLAS object, we first retrieved every matching APOP source within a radius of 30 arcsec (typically four to eight objects) and compared the modified Julian date (MJD) of the ATLAS observation with that of APOP (by definition at epoch J2000 so MJD 51544). We defined an epoch difference $\Delta t = \text{MJD}_{\text{ATLAS}} - 51544$ and then used the proper motions and J2000 positions from APOP to compute predicted positions at the epoch of the ATLAS imaging for all objects in the first cross-match (Fig. 4). This coordinate ‘forward projection’ is carried out according to

$$\alpha = \alpha_{\text{APOP}} + \left(\frac{\mu_{\alpha}}{\cos(\delta_{\text{APOP}})} \right) \times \frac{\Delta t}{365.25}, \quad (2)$$

$$\delta = \delta_{\text{APOP}} + \mu_{\delta} \times \frac{\Delta t}{365.25}, \quad (3)$$

where μ_{α} and μ_{δ} are the objects proper motions in right ascension and declination, respectively. Finally, we consider a true match to be the closest object whose forward projected coordinates fall within 2 arcsec of the ATLAS ones. In cases where more than one matching object is found within 2 arcsec (a few tens within the entire sample), we select the best match by visually inspecting the magnitudes of the matching pairs and their angular separation.

Following this procedure, we obtained proper motions for 11 407 objects. The most likely explanation for the 952 ATLAS objects for which we could not find a counterpart in APOP is that they could not be reliably matched up on the photographic plates used by APOP.

¹ as defined on the quality bit flags description at <http://osa.roe.ac.uk>.

Table 2. SQL casjob flags used to select ATLAS point sources with reliable photometry from the OmegaCAM Science Archive webpage.

Constraint	Effect
(mergedClass = -1) OR (mergedClass = -2)	selects objects marked as ‘stellar’ or ‘probable stellar’
AND (uppErrBits gppErrBits rppErrBits ippErrBits zppErrBits) < 65536	exclude sources with any ‘important’ quality issues
OR (uppErrBits gppErrBits rppErrBits ippErrBits zppErrBits) & 0x00400040 != 0	does not exclude ‘source within a dither offset of the stacked frame boundary’

Table 3. Equations describing the colour and magnitude constraints used to select sources in the ATLAS footprint. The colour cuts were applied to the ATLAS magnitudes after converting them into SDSS equivalent ones.

Colour	Constraint
$(u - g)$	$\leq 3.917 \times (g - r) + 2.344$
$(u - g)$	$\leq 0.098 \times (g - r) + 0.721$
$(u - g)$	$\geq 1.299 \times (g - r) - 0.079$
$(g - r)$	≤ 0.450
$(g - r)$	$\geq 2.191 \times (r - i) - 0.638$
$(r - i)$	$\leq -0.452 \times (i - z) + 0.282$
g	≤ 19

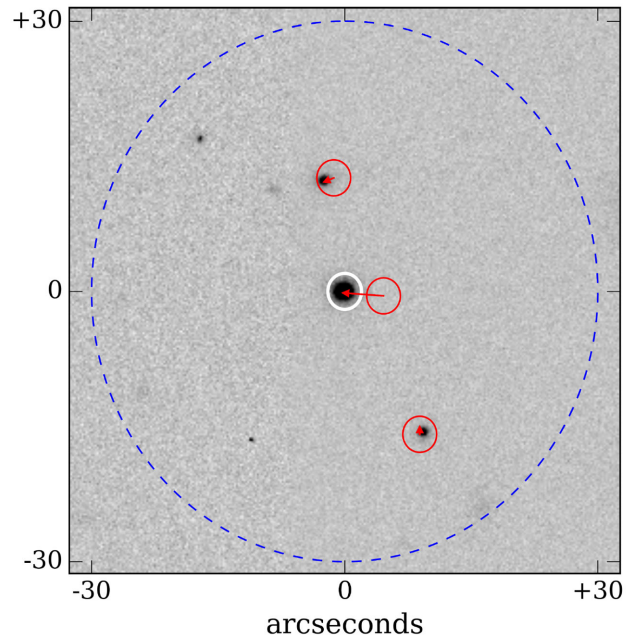
5 WHITE DWARF CANDIDATES SELECTION

In order to identify reliable white dwarf candidates among ATLAS sources, we rely on the photometric selection method presented in Gentile Fusillo et al. (2015a) that can be used to assign a ‘probability of being a white dwarf’ (P_{WD}) to any object with available multiband photometry and proper motion. In this section, we briefly summarize the details of the selection method; for a full description refer to Gentile Fusillo et al. (2015a). The P_{WD} values rely on a probability map that traces the distribution of spectroscopically confirmed white dwarfs and contaminant objects selected from SDSS in colour and reduced proper motion H computed as

$$H_g = g + 5 \log \mu + 5, \quad (4)$$

where μ is the proper motion in arcsec yr^{-1} . This probability map effectively traces which areas in colour- H space are more likely populated by either white dwarfs or contaminants. In our work on SDSS photometry, we determined that the strongest discrimination between white dwarfs and contaminants is obtained in the $g - z$, H_g space, which we therefore adopted for our selection method. The final map was constructed using a training sample of over 27 000 objects (different types of white dwarfs, quasars and stellar contaminants) that were classified by visual inspection of their SDSS spectra. By combining the $(g - z, H_g)$ position of a test object with this probability map, we can compute a quantity that directly indicates how likely it is for the object to be a white dwarf, in other words our P_{WD} . We have shown above that ATLAS_{SDSS} magnitudes are equivalent to the SDSS ones. We therefore calculated H_g for all ATLAS objects using the ATLAS_{SDSS} magnitudes and the APOP proper motions, and directly applied the Gentile Fusillo et al. (2015a) selection method to calculate P_{WD} for all 11 407 ATLAS sources in our sample. In Table 4, we summarize the content of our final catalogue of ATLAS white dwarf candidates.

We also performed a cross-match of our catalogue with the *Gaia* DR1 source catalogue (Gaia Collaboration et al. 2016) and provide *Gaia* source ID and G -band mean magnitude for all matching sources. *Gaia* is able to resolve objects with a sky separation of

**Figure 4.** ATLAS g -band image centred at the position of one of our white dwarf candidates. The blue circle represents the 30 arcsec radius area used for the first cross-match with APOP. 2 arcsec radius circles are shown centred on the J2000 APOP coordinates of all matching sources in the initial cross-match and the red arrows indicate how the objects moved between J2000 and the ATLAS epoch of observation. The white circle indicates the final 2 arcsec matching radius around the ATLAS source.

0.23 arcsec (de Bruijne et al. 2015), a resolution much higher than what is achievable by VST ground based observations. As a result, we found two ATLAS objects (ATLASJ235435.65–290704.08 and ATLASJ121100.93–075241.23) that were each matched to two *Gaia* sources both with an angular separation of < 1 arcsec. These objects are likely to be binary systems that were resolved with *Gaia*, but not in ATLAS. ATLASJ121100.93–075241.23 could be of particular interest being a relatively bright white dwarf candidate ($P_{WD} = 0.71$, $g = 15.9$) with a potential faint close companion ($G = 18.4$). Out of the five ATLAS bands, we find that r is the one closest to *Gaia* G particularly for sources with $g - r \geq 0$ where the mean difference $G - r$ is 0.12 mag.

6 DISCUSSION

6.1 Comparison with SDSS

In Gentile Fusillo et al. (2015a), we used an independent sample of spectroscopically confirmed white dwarfs and contaminants from SDSS DR9 and DR10 and later LAMOST DR3 (Gentile Fusillo

Table 4. Format of the catalogue of VST ATLAS white dwarfs candidates. The full catalogue can be accessed online via VizierR.

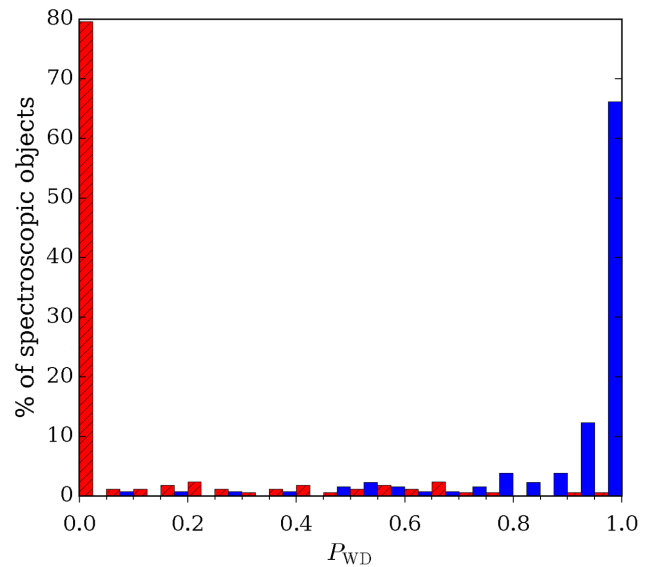
Column no.	Heading	Description
1	VST ATLAS name	ATLAS objects name (ATLAS + J2000 coordinates)
2	ATLAS ID	Unique ID identifying the photometric source in ATLAS
3	ra	Right ascension
4	dec	Declination
5	P_{WD}	The <i>probability of being a WD</i> computed for this object
6	umag	ATLAS <i>u</i> -band magnitude
7	umag err	ATLAS <i>u</i> -band magnitude uncertainty
8	gmag	ATLAS <i>g</i> band magnitude
9	gmag err	ATLAS <i>g</i> -band magnitude uncertainty
10	rmag	ATLAS <i>r</i> band magnitude
11	rmag err	ATLAS <i>r</i> -band magnitude uncertainty
12	imag	ATLAS <i>i</i> -band magnitude
13	imag err	ATLAS <i>i</i> -band magnitude uncertainty
14	zmag	ATLAS <i>z</i> -band magnitude
15	zmag err	ATLAS <i>z</i> -band magnitude uncertainty
16	MJD	Modified julian date of ATLAS observation
17	pmra	APOP proper motion in right ascension (mas yr^{-1})
18	pmra err	APOP proper motion in right ascension uncertainty (mas yr^{-1})
19	pmdec	APOP proper motion in declination (mas yr^{-1})
20	pmdec err	APOP proper motion in declination uncertainty (mas yr^{-1})
21	human class	Classification of the object based on inspection of its available spectrum (section 6.2)
22	Simbad type1	Currently available primary Simbad classifications
23	Simbad type2	Currently available secondary Simbad classifications
24	Gaia ID	<i>Gaia</i> DR1 source ID
25	Gmag	<i>Gaia</i> DR1 <i>G</i> -band mean magnitude

et al. 2015b) to demonstrate the efficiency of the selection method and the completeness of our catalogue of SDSS white dwarf candidates. However, similarly large spectroscopic samples do not exist for the Southern hemisphere and therefore we cannot test in the same way the robustness of the selection method when applied to ATLAS photometry. None the less, as a result of the overlap of ATLAS with SDSS, 879 objects appear in both the Gentile Fusillo et al. (2015a) catalogue of SDSS white dwarf candidates and in the ATLAS catalogue presented here. This sample includes 130 white dwarfs and 171 contaminants confirmed by SDSS spectroscopy (as of SDSS DR12 Alam et al. 2015) that enable us to carry out some valuable tests on the ATLAS sample of white dwarf candidates.

Fig. 5 shows that the vast majority of the 130 white dwarfs have $P_{WD}(\text{ATLAS}) > 0.8$ while over 85 per cent of the 171 contaminants have $P_{WD}(\text{ATLAS}) < 0.2$. Though this test is limited to small sample sizes, it is evident that the P_{WD} calculated from ATLAS and APOP data provide a clear discrimination between white dwarfs and contaminants.

Using the same spectroscopic sample, we can also calculate that a confidence cut that includes all ATLAS objects with $P_{WD} \geq 0.41$ results in a 96 per cent completeness and 87 per cent efficiency in selecting white dwarfs. These numbers are very similar to those obtained from the catalogue of SDSS white dwarf candidates (Gentile Fusillo et al. 2015a) when applying the same cut in P_{WD} . We also compared the surface density of ATLAS and SDSS white dwarf candidates with $P_{WD} \geq 0.41$, and for both samples, we find an average of $\simeq 1.8$ objects per deg^2 . These results suggest that our catalogue of ATLAS white dwarf candidates should be as complete and reliable as the SDSS catalogue presented in Gentile Fusillo et al. (2015a).

The common ATLAS and SDSS white dwarf candidates also allow us to directly compare P_{WD} values calculated using ATLAS and APOP with those calculated using SDSS data. We find that the P_{WD} values are largely consistent with an average difference $|P_{WD}(\text{ATLAS}) - P_{WD}(\text{SDSS})| = 0.042 \pm 0.03$.

**Figure 5.** Distribution of 301 spectroscopically confirmed white dwarfs (blue) and contaminants (red, shaded) from the SDSS and ATLAS overlap sample as a function of P_{WD} .

However, $\simeq 4$ per cent of the objects in the overlapping SDSS and ATLAS sample show significantly inconsistent P_{WD} values, $|P_{WD}(\text{ATLAS}) - P_{WD}(\text{SDSS})| \geq 0.2$. Close inspection of these objects reveals that the cause of such difference in P_{WD} is a marked discrepancy in the SDSS and APOP proper motions, potentially caused by erroneous matching on the original photographic plates used by the surveys. Additionally, despite our best efforts, we cannot fully exclude that a limited number of ATLAS objects may have been matched to the wrong APOP object (see Section 4) leading to a wrong assumed proper motion. Even accounting for this

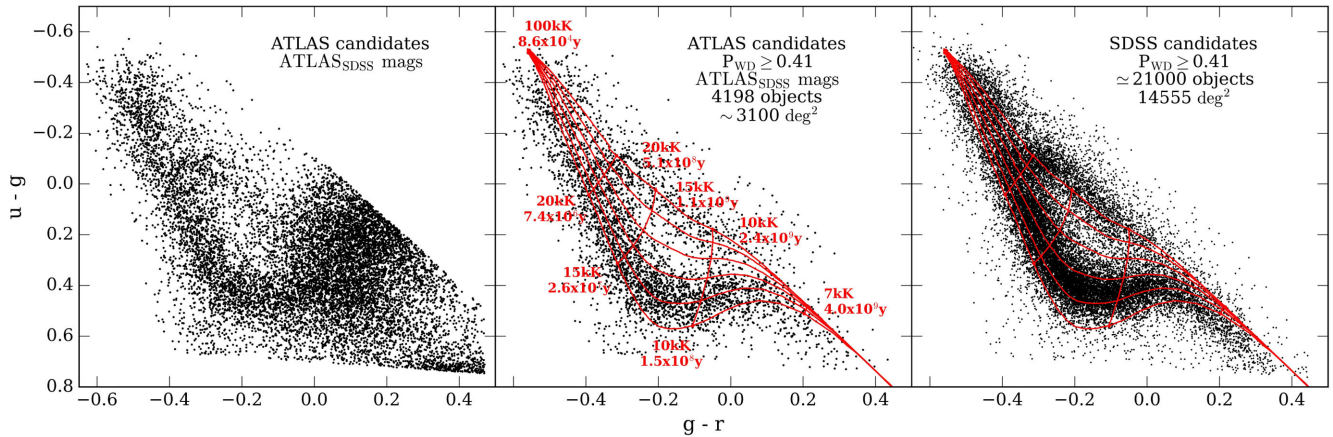


Figure 6. $u - g$, $g - r$ colour-colour distribution of (from left- to right-hand side): all 11 407 ATLAS objects in our final sample; 4205 ATLAS objects with $P_{WD} \geq 0.41$; $\simeq 21000$ white dwarf candidates from Gentile Fusillo et al. (2015a) with $P_{WD} \geq 0.41$ for comparison. White dwarf cooling tracks from Holberg & Bergeron (2006) are shown in red overlay.

small number of inconsistencies, we are confident that the P_{WD} values calculated can be used to reliably select high-confidence dwarf candidates, i.e. Fig. 6 clearly illustrate that the colour-colour distribution of the ATLAS $P_{WD} \geq 0.41$ sample is remarkably similar to that of the equivalent sample selected from the Gentile Fusillo et al. (2015a) SDSS catalogue. Taking into account the values of completeness and efficiency calculated before, we estimate that our catalogue contains $\simeq 4100$ high-confidence white dwarf candidates.

6.2 Spectroscopic follow-up

To further test the reliability of our selection method, we obtained spectra for a total of 185 objects from our catalogue. 169 objects were observed with the two degree field (‘2dF’) multi-object system of the AAOmega spectrograph on the Anglo Australia Telescope (AAT). These spectra were acquired as part of the 2dF Quasar Dark Energy Survey pilot (Chehade et al. 2016). The observations were made using the 580V and 385R gratings for the blue and red arm of the spectrograph, respectively. This configuration achieves a useful wavelength range between 3700 and 8800 Å. The data reduction was carried out using the 2dFDR² data reduction pipeline (for more details see Chehade et al. 2016). Among these 169 targets, we identified 14 new white dwarfs, all of which have $P_{WD} > 0.7$. The remaining objects are mostly quasars with $P_{WD} < 0.2$ and only four of them have $P_{WD} > 0.45$.

We also selected 16 additional targets specifically as high-confidence white dwarf candidates ($P_{WD} \geq 0.85$) and observed them with the New Technology Telescope (NTT) and the VLT as part of backup programs due to a northern pointing restriction for strong northerly winds. 13 targets were observed on 2015 September 16 using the EFOSC2 instrument on the NTT at la Silla, Chile with the ‘Gr#7’ grism and a 1-arcsec slit, and with exposure times in the range of 300–900 s. We carried out optimal spectral reduction and calibration using the packages PAMELA³ and MOLLY⁴ (Marsh 1989). The last three objects were observed on 2015 September 24 at the VLT observatory with the X-Shooter spectrograph, using a 1-arcsec

slit for the UVB arm and 0.9-arcsec for the VIS arm and exposure times of ~ 1500 s. The spectra were reduced using the standard procedures within the REFLEX⁵ reduction tool developed by ESO. All 16 high-confidence white dwarf candidates were confirmed as white dwarfs (Table 5). Both the NTT and the VLT observations were undertaken as backup programs due to a northern pointing restrfor strong northerly winds.

6.3 Spectral analysis

Of the 30 new spectroscopically confirmed white dwarfs, 27 stars have hydrogen-dominated atmospheres (DA), one shows strong Ca H&K lines (DZ, Fig. 7), one has a likely carbon-dominated atmosphere (DQ) and another star does not show strong atmospheric features at the signal-to-noise level of the spectrum we obtained. Two DA white dwarfs display also Zeeman splitting of the hydrogen lines due to moderately strong magnetic fields (DAH, e.g. Fig. 7).

In Table 5, we summarize the spectral classification and we report the atmospheric parameters (T_{eff} , $\log g$) of the DA white dwarfs, which we have measured through comparison with a grid of Koester (2010) model spectra (Fig. 8). The synthetic spectra were computed with the mixing-length prescription of $ML2/\alpha = 0.8$, and include the Stark broadening profiles by Tremblay & Bergeron (2009). For the spectral analysis, we used FITSB2 (Napiwotzki et al. 2004) that determines the best-fitting model via χ^2 minimization of the Balmer line profiles for observed and synthetic spectra, using a downhill simplex algorithm (e.g. the AMOEBA routine; Press et al. 1992) and a bootstrap method to assess the uncertainties. For cool DA white dwarfs ($T_{\text{eff}} < 15\,000$ K), we applied the Tremblay et al. (2013) 3D corrections of the atmospheric parameters to account for the inaccurate treatment of convection in 1D models.

The spectroscopic parameters are broadly consistent with the photometric estimates one would derive from comparison with the white dwarf cooling sequences (Fig. 6).

6.4 New pulsating white dwarfs

As it continues its tour around the ecliptic plane, the extended *Kepler* mission (K2) has opened the possibility to observe many new

² <http://www.aao.gov.au/science/software/2dfdr>

³ PAMELA was written by T. R. Marsh and can be found in the STARLINK distribution Hawaiiki and later releases.

⁴ MOLLY was written by T. R. Marsh and is available from <http://www.warwick.ac.uk/go/trmarsh/software>.

⁵ <http://www.eso.org/sci/software/reflex/>

Table 5. List of ATLAS white dwarf candidates confirmed by spectroscopic observations. For DA white dwarfs, we also report the T_{eff} and $\log g$ from the best-fitting model adjusted using the Tremblay et al. (2013) 3D corrections. Spectral-type classification with the ‘:’ suffix is considered uncertain due to the low quality of the spectrum.

Name	RA	Dec.	P_{WD}	Instrument	Type	T_{eff} (K)	$\log g$
ATLAS J034131.17–272144.73	55.379 88	– 27.362 427	0.95	X-Shooter	DA	$13\,519 \pm 450$	7.81 ± 0.07
ATLAS J001618.70–343056.17	4.077 932	– 34.515 605	0.98	X-Shooter	DA	$11\,329 \pm 160$	7.72 ± 0.05
ATLAS J000119.76–394703.17	0.332 369	– 39.784 214	0.99	X-Shooter	DA	$12\,684 \pm 310$	8.10 ± 0.08
ATLAS J000344.78–391523.32	0.936 586	– 39.256 48	0.89	EFOSC2	DA	6946 ± 100	7.28 ± 0.27
ATLAS J002239.01–311039.05	5.662 562	– 31.177 516	1.00	EFOSC2	DAH		
ATLAS J002606.30–322423.70	6.526 252	– 32.406 585	0.99	EFOSC2	DA	$11\,708 \pm 150$	8.10 ± 0.05
ATLAS J014005.85–344724.11	25.024 40	– 34.790 033	0.96	EFOSC2	DA	$11\,721 \pm 630$	7.76 ± 0.28
ATLAS J023320.65–320310.88	38.336 047	– 32.053 023	0.99	EFOSC2	DA	$10\,770 \pm 180$	7.99 ± 0.06
ATLAS J023752.56–304133.16	39.469 012	– 30.692 547	0.99	EFOSC2	DAH		
ATLAS J034356.22–334106.29	55.984 261	– 33.685 081	0.96	EFOSC2	DA	$12\,419 \pm 420$	8.37 ± 0.09
ATLAS J214039.37–341920.25	325.164 068	– 34.322 294	0.96	EFOSC2	DA	$17\,140 \pm 230$	7.85 ± 0.06
ATLAS J220217.30–391728.36	330.572 104	– 39.291 212	0.98	EFOSC2	DA	9508 ± 90	7.94 ± 0.08
ATLAS J222337.44–343839.72	335.906 028	– 34.644 369	0.87	EFOSC2	DZ		
ATLAS J224510.44–383645.71	341.293 532	– 38.612 699	0.88	EFOSC2	DA	$10\,194 \pm 290$	7.85 ± 0.10
ATLAS J224653.56–385651.24	341.723 203	– 38.947 567	1.00	EFOSC2	DAV	$10\,432 \pm 290$	8.06 ± 0.10
ATLAS J230223.57–114811.36	345.598 21	– 11.803 158	0.98	EFOSC2	DA	$10\,077 \pm 140$	7.92 ± 0.06
ATLAS J034255.41–300122.62	55.730 916	– 30.022 952	0.99	2dF	DA	$15\,270 \pm 980$	9.13 ± 0.22
ATLAS J033004.84–295300.07	52.520 199	– 29.883 353	0.97	2dF	DA	$17\,880 \pm 640$	8.06 ± 0.12
ATLAS J034456.50–265224.69	56.235 429	– 26.873 526	0.93	2dF	DA	$35\,860 \pm 1150$	8.51 ± 0.21
ATLAS J034922.82–254709.30	57.345 107	– 25.785 918	0.72	2dF	DA	7648 ± 110	7.56 ± 0.24
ATLAS J035010.83–261739.46	57.545 143	– 26.294 295	0.90	2dF	DA:		
ATLAS J121646.04–062443.49	184.191 856	– 6.412 081	0.96	2dF	DA	7694 ± 230	7.85 ± 0.81
ATLAS J121655.61–063810.24	184.231 716	– 6.636 178	0.75	2dF	DA	9366 ± 270	8.33 ± 0.27
ATLAS J121844.60–064243.39	184.685 854	– 6.712 053	0.99	2dF	DA	$19\,750 \pm 760$	7.66 ± 0.15
ATLAS J123540.68–074802.08	188.919 502	– 7.800 578	0.99	2dF	DA	7950 ± 230	6.24 ± 0.94
ATLAS J132001.63–074703.50	200.006 82	– 7.784 306	0.99	2dF	DA	$14\,690 \pm 1190$	8.41 ± 0.19
ATLAS J152811.82–145839.45	232.049 259	– 14.977 627	0.99	2dF	DQ:		
ATLAS J234049.50–314633.67	355.206 261	– 31.776 022	0.96	2dF	DA	9568 ± 100	7.99 ± 0.09
ATLAS J234332.65–311950.08	355.886 063	– 31.330 578	0.96	2dF	DA	$13\,240 \pm 340$	8.08 ± 0.09
ATLAS J121912.39–071436.07	184.801 635	– 7.243 353	0.99	2dF	DC:		
ATLAS J134211.62–073540.1	205.548 443	– 7.594 483	1.00	SOAR	DA	$11\,190 \pm 170$	8.02 ± 0.05

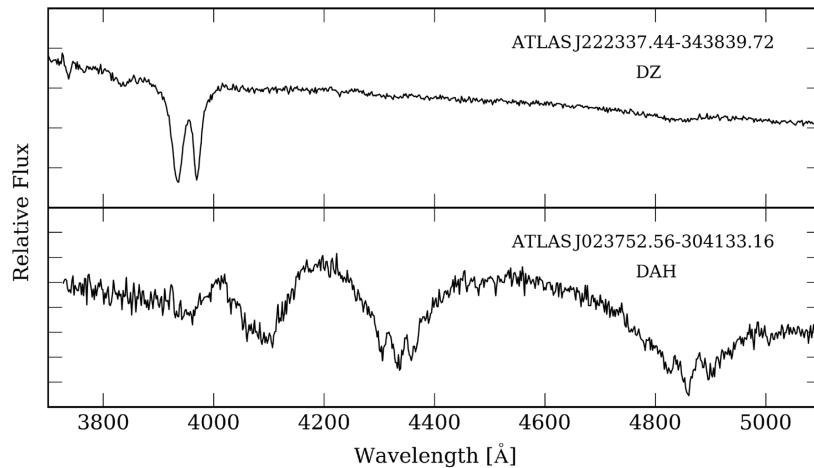


Figure 7. Spectra of the DZ white dwarf and of one magnetic white dwarfs discovered by follow-up observations of candidates using EFOSC2.

white dwarfs, especially those that pulsate. We have utilized this catalogue of candidate white dwarfs from ATLAS for target selection of several Guest Observer proposals (for Field 6, 12 and 15 in *K2* Campaign 6). One of our candidates, selected solely based on its P_{WD} and ATLAS *ugr* colours, was observed to pulsate: ATLASJ134211.62–073540.1 (EPIC 229227292). In fact, this star became the fourth white dwarf to show aperiodic, large-amplitude outbursts in its *K2* observations (Bell et al. 2016). Follow-up

spectroscopy from the Southern Astrophysical Research (SOAR) telescope confirmed this is a DA white dwarf with atmospheric parameters corresponding to $11\,190 \pm 170$ K, $\log g = 8.02 \pm 0.05$, $M_{\text{WD}} = 0.62 \pm 0.03$. This is now the second-brightest white dwarf known to show such outbursts, which may arise result from a parametric resonant coupling (Hermes et al. 2015).

Additionally, several of the white dwarfs analysed in Table 5 have temperatures and gravities near the empirical DAV instability

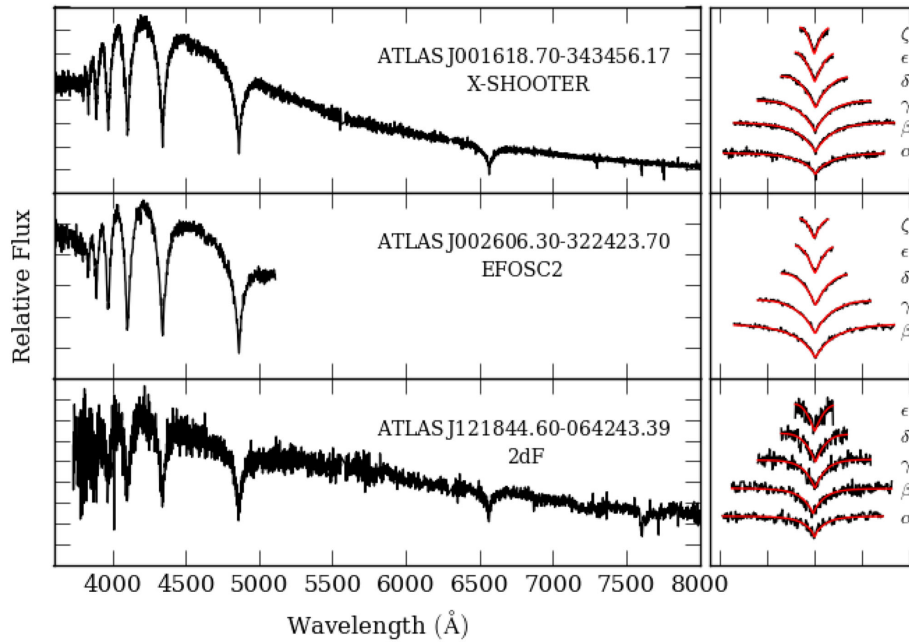


Figure 8. Sample spectra of three white dwarf candidates confirmed by observations with X-SHOOTER, EFOSC2 and 2dF. The panels on the right show the best-fitting models overlaid on the normalized Balmer lines used for the fit.

strip. We followed-up four of these stars with high-speed photometry from the SOAR at Cerro Pachon in Chile. All targets were observed with the Goodman spectrograph in imaging mode using 20 s exposures through an S8612 filter. Three of the observed white dwarfs do not show photometric variability, with good limits on a lack of pulsations. ATLASJ023320.65–320310.88 was observed for 2.0 h and does not vary to a limit of 0.8 ppt (1 ppt = 0.1 per cent). ATLASJ214039.37–341920.25 was observed for 2.4 h and does not vary to a limit of 2.0 ppt. ATLASJ224510.44–383645.71 was observed for 2.1 h and does not vary to a limit of 2.9 ppt. However, we have detected significant variability in a 1.8 h run on ATLAS224653.56–385651.24: a 4.9(3) ppt peak at 1502.0 ± 10.3 s. If confirmed, this would be one of the coolest (and longest-period) pulsating white dwarfs detected to date. Within the uncertainties in T_{eff} and $\log g$ (Table 5), the two pulsating white dwarfs can be placed inside of the empirical ZZ Ceti instability strip and similarly the three stars observed not to vary can be placed outside it.

7 CONCLUSION

We presented the application of our selection method for photometric white dwarfs candidates (Gentile Fusillo et al. 2015a) to the latest internal data release of the VST ATLAS survey combined with proper motions from APOP. The resulting catalogue contains 11 407 ATLAS sources with computed P_{WD} . Using a small number of SDSS spectroscopically confirmed white dwarfs and contaminants, we calculated that a confidence cut at $P_{\text{WD}} \geq 0.41$ produces a sample of white dwarfs that is 96 per cent complete with an efficiency of 87 per cent. We estimate that our catalogue contains $\simeq 4200$ high-confidence white dwarf candidates the majority of which have not yet received spectroscopic follow-up. Only ~ 15 per cent of the white dwarfs known to date are located in the Southern hemisphere and our catalogue therefore constitute a significant improvement on the current north–south knowledge gap.

Among these thousands of new white dwarfs, we expect to find several systems of particular interest: metal polluted white dwarfs

(most likely more than 1000 in the final ATLAS footprint) that will improve current statistics on planetary debris abundances, a few tens of white dwarfs with detectable debris discs that can be identified combining our catalogue with IR data from the Vista Hemisphere Survey (VHS, McMahon et al. 2013) and WISE (Wright et al. 2010), several magnetic white dwarfs and white dwarfs with rare atmospheric composition (e.g. DQ) like those already identified in our limited spectroscopic follow-up (Section 6.2) and more pulsating white dwarfs (Section 6.4). The application of our catalogue to most white dwarfs population studies will ultimately require spectroscopic follow-up. The possibility to rely on the P_{WD} s allows one to tailor future spectroscopic observations prioritising efficiency (and therefore high P_{WD} targets) for single target observations or completeness in large scale campaigns.

ACKNOWLEDGEMENTS

We thank the anonymous referee for the fast and constructive comments received. The research leading to these results has received funding from the European Research Council under the European Union’s Seventh Framework Programme (FP/2007-2013)/ERC Grant Agreement n.320964 (WDTracer). Support for this work was provided by NASA through a Hubble Fellowship grant HST-HF2-51357.001-A. This paper is based on observations made with ESO Telescopes at the Paranal Observatory under programme ID 095.D-0406(B), 095.D-0802(B), 097.D-1029(A), 177.A-3011 (A-I) and also based on observations obtained at the Southern Astrophysical Research (SOAR) telescope, which is a joint project of the Ministério da Ciência, Tecnologia, e Inovação da República Federativa do Brasil, the U.S. National Optical Astronomy Observatory, the University of North Carolina at Chapel Hill and Michigan State University. Funding for SDSS-III has been provided by the Alfred P. Sloan Foundation, the Participating Institutions, the National Science Foundation and the U.S. Department of Energy Office of Science. The SDSS-III website is <http://www.sdss3.org/>. SDSS-III is managed by the Astrophysical Research Consortium for the

Participating Institutions of the SDSS-III Collaboration including the University of Arizona, the Brazilian Participation Group, Brookhaven National Laboratory, Carnegie Mellon University, University of Florida, the French Participation Group, the German Participation Group, Harvard University, the Instituto de Astrofísica de Canarias, the Michigan State/Notre Dame/JINA Participation Group, Johns Hopkins University, Lawrence Berkeley National Laboratory, Max Planck Institute for Astrophysics, Max Planck Institute for Extraterrestrial Physics, New Mexico State University, New York University, Ohio State University, Pennsylvania State University, University of Portsmouth, Princeton University, the Spanish Participation Group, University of Tokyo, University of Utah, Vanderbilt University, University of Virginia, University of Washington and Yale University.

Facilities: VST, AAT, NTT, VLT, SOAR, SDSS

REFERENCES

- Alam S. et al., 2015, *ApJ*, 219, 12
 Bell K. J. et al., 2016, *ApJ*, 829, 82
 Bergeron P., Saffer R. A., Liebert J., 1992, *ApJ*, 394, 228
 Brown W. R., Kilic M., Allende Prieto C., Kenyon S. J., 2010, *ApJ*, 723, 1072
 Castanheira B. G. et al., 2004, *A&A*, 413, 623
 Catalán S., Isern J., García-Berro E., Ribas I., 2008, *MNRAS*, 387, 1693
 Chehade B. et al., 2016, *MNRAS*, 459, 1179
 de Bruijne J. H. J., Allen M., Azaz S., Krone-Martins A., Prod'homme T., Hestroffer D., 2015, *A&A*, 576, A74
 de Jong J. T. A. et al., 2013, *The Messenger*, 154, 44
 Debes J. H., Hoard D. W., Wachter S., Leisawitz D. T., Cohen M., 2011, *ApJ*, 197, 38
 Drew J. E. et al., 2014, *MNRAS*, 440, 2036
 Dufour P. et al., 2007, *ApJ*, 663, 1291
 Dufour P., Kilic M., Fontaine G., Bergeron P., Lachapelle F., Kleinman S. J., Leggett S. K., 2010, *ApJ*, 719, 803
 Eisenstein D. J. et al., 2006, *ApJS*, 167, 40
 Falcon R. E., Winget D. E., Montgomery M. H., Williams K. A., 2010, *ApJ*, 712, 585
 Farihi J., Becklin E. E., Zuckerman B., 2005, *ApJS*, 161, 394
 Farihi J., Jura M., Zuckerman B., 2009, *ApJ*, 694, 805
 Gaia Collaboration et al., 2016, *A&A*, 595, A2
 Gänsicke B. T., Euchner F., Jordan S., 2002, *A&A*, 394, 957
 Gänsicke B. T., Marsh T. R., Southworth J., Rebassa-Mansergas A., 2006, *Science*, 314, 1908
 Gänsicke B. T., Koester D., Girven J., Marsh T. R., Steeghs D., 2010, *Science*, 327, 188
 Gentile Fusillo N. P. et al., 2015b, *MNRAS*, 452, 765
 Gentile Fusillo N. P., Gänsicke B. T., Greiss S., 2015a, *MNRAS*, 448, 2260
 Gentile Fusillo N. P., Hermes J. J., Gänsicke B. T., 2016, *MNRAS*, 455, 2295
 Giammichele N., Bergeron P., Dufour P., 2012, *ApJ*, 199, 29
 Girven J., Gänsicke B. T., Steeghs D., Koester D., 2011, *MNRAS*, 417, 1210
 Greiss S., Gänsicke B. T., Hermes J. J., Steeghs D., Koester D., Ramsay G., Barclay T., Townsley D. M., 2014, *MNRAS*, 438, 3086
 Harris H. C. et al., 2003, *AJ*, 126, 1023
 Hermes J. J. et al., 2014, *ApJ*, 792, 39
 Hermes J. J. et al., 2015, *ApJ*, 810, L5
 Holberg J. B., Bergeron P., 2006, *AJ*, 132, 1221
 Holberg J. B., Oswalt T. D., Sion E. M., 2002, *ApJ*, 571, 512
 Holberg J. B., Sion E. M., Oswalt T., McCook G. P., Foran S., Subasavage J. P., 2008, *AJ*, 135, 1225
 Hollands M. A., Gänsicke B. T., Koester D., 2015, *MNRAS*, 450, 681
 Iben I. J., Ritossa C., Garcia-Berro E., 1997, *ApJ*, 489, 772
 Kepler S. O. et al., 2013, *MNRAS*, 429, 2934
 Kepler S. O. et al., 2015, *MNRAS*, 446, 4078
 Kepler S. O. et al., 2016, *MNRAS*, 455, 3413
 Kepler S. O., Koester D., Ourique G., 2016, *Science*, 352, 67
 Kleinman S. J. et al., 2013, *ApJS*, 204, 5
 Koester D., 2010, *Mem. Soc. Astron. Ital.*, 81, 921
 Koester D., Gänsicke B. T., Farihi J., 2014, *A&A*, 566, A34
 Kuijken K., 2011, *The Messenger*, 146, 8
 Külebi B., Jordan S., Euchner F., Gänsicke B. T., Hirsch H., 2009, *A&A*, 506, 1341
 Lasker B. M., STSCI Sky-Survey Team, 1998, *BAAS*, 30, 912
 Liebert J., Bergeron P., Holberg J. B., 2005, *ApJS*, 156, 47
 Manser C. J. et al., 2016, *MNRAS*, 455, 4467
 Marsh T. R., 1989, *PASP*, 101, 1032
 Marsh T. R., Nelemans G., Steeghs D., 2004, *MNRAS*, 350, 113
 McMahon R. G., Banerji M., Gonzalez E., Koposov S. E., Bejar V. J., Lodieu N., Rebolo R., VHS Collaboration, 2013, *The Messenger*, 154, 35
 Napiwotzki R. et al., 2004, in Hilditch R. W., Hensberge H., Pavlovski K., eds., *ASP Conf. Ser. Vol. 318, Spectroscopically and Spatially Resolving the Components of the Close Binary Stars*. Astron. Soc. Pac., San Francisco, p. 402
 Parsons S. G., Marsh T. R., Gänsicke B. T., Drake A. J., Koester D., 2011, *ApJ*, 735, L30
 Press W. H., Teukolsky S. A., Vetterling W. T., Flannery B. P., 1992, *Numerical recipes in FORTRAN. The Art of Scientific Computing*. Cambridge Univ. Press, Cambridge
 Qi Z. et al., 2015, *AJ*, 150, 137
 Raddi R., Gänsicke B. T., Koester D., Farihi J., Hermes J. J., Scaringi S., Breedt E., Girven J., 2015, *MNRAS*, 450, 2083
 Raddi R. et al., 2016, *MNRAS*, 457, 1988
 Rebassa-Mansergas A. et al., 2015, *MNRAS*, 450, 743
 Schipani P. et al., 2012, in Stepp L. M., Gilmozzi R., Hall H. J., eds., *Proc. SPIE Conf. Ser. Vol. 8444, Ground-based and Airborne Telescopes IV*. SPIE, Bellingham, p. 84441C
 Schmidt G. D., Liebert J., Harris H. C., Dahn C. C., Leggett S. K., 1999, *ApJ*, 512, 916
 Schmidt G. D. et al., 2003, *ApJ*, 595, 1101
 Shanks T. et al., 2015, *MNRAS*, 451, 4238
 Sion E. M., Leckenby H. J., Szkody P., 1990, *ApJ*, 364, L41
 Sion E. M., Holberg J. B., Oswalt T. D., McCook G. P., Wasatonic R., Myszka J., 2014, *AJ*, 147, 129
 Steele P. R. et al., 2013, *MNRAS*, 429, 3492
 Torres S., García-Berro E., Isern J., Figueras F., 2005, *MNRAS*, 360, 1381
 Tremblay P.-E., Bergeron P., 2009, *ApJ*, 696, 1755
 Tremblay P.-E., Ludwig H.-G., Steffen M., Freytag B., 2013, *A&A*, 552, A13
 Tremblay P.-E., Kalirai J. S., Soderblom D. R., Cignoni M., Cummings J., 2014, *ApJ*, 791, 92
 Tremblay P.-E., Cummings J., Kalirai J. S., Gänsicke B. T., Gentile-Fusillo N., Raddi R., 2016, *MNRAS*, 461, 2100
 Vennes S., Kawka A., 2008, *MNRAS*, 389, 1367
 Wilson D. J., Gänsicke B. T., Koester D., Raddi R., Breedt E., Southworth J., Parsons S. G., 2014, *MNRAS*, 445, 1878
 Wright E. L. et al., 2010, *AJ*, 140, 1868
 York D. G. et al., 2000, *AJ*, 120, 1579
 Zuckerman B., Reid I. N., 1998, *ApJ*, 505, L143

SUPPORTING INFORMATION

Supplementary data are available at [MNRAS](https://www.mnras.org) online.

Table 4. Format of the catalogue of VST ATLAS white dwarfs candidates. The full catalogue can be accessed online via VizieR.

Please note: Oxford University Press is not responsible for the content or functionality of any supporting materials supplied by the authors. Any queries (other than missing material) should be directed to the corresponding author for the article.

This paper has been typeset from a \LaTeX file prepared by the author.